

1 Spectral Properties of Bright Fermi-detected Blazars in the Gamma-ray Band

2 A. A. Abdo^{1,2}, M. Ackermann³, M. Ajello³, W. B. Atwood⁴, M. Axelsson^{5,6}, L. Baldini⁷,
 3 J. Ballet⁸, G. Barbiellini^{9,10}, D. Bastieri^{11,12}, K. Bechtol³, R. Bellazzini⁷, B. Berenji³,
 4 R. D. Blandford³, E. D. Bloom³, E. Bonamente^{13,14}, A. W. Borgland³, A. Bouvier³, J. Bregeon⁷,
 5 A. Brez⁷, M. Brigida^{15,16}, P. Bruel¹⁷, T. H. Burnett¹⁸, S. Buson¹¹, G. A. Caliendo¹⁹,
 6 R. A. Cameron³, P. A. Caraveo²⁰, S. Carrigan¹², J. M. Casandjian⁸, E. Cavazzuti²¹,
 7 C. Cecchi^{13,14}, Ö. Çelik^{22,23,24}, E. Charles³, A. Chekhtman^{1,25}, C. C. Cheung^{1,2}, J. Chiang³,
 8 S. Ciprini¹⁴, R. Claus³, J. Cohen-Tanugi²⁶, J. Conrad^{27,6,28}, S. Cutini²¹, C. D. Dermer¹,
 9 A. de Angelis²⁹, F. de Palma^{15,16}, S. W. Digel³, E. do Couto e Silva³, P. S. Drell³, R. Dubois³,
 10 D. Dumora^{30,31}, C. Farnier²⁶, C. Favuzzi^{15,16}, S. J. Fegan¹⁷, W. B. Focke³, P. Fortin¹⁷,
 11 M. Frailis^{29,32}, Y. Fukazawa³³, S. Funk³, P. Fusco^{15,16}, F. Gargano¹⁶, D. Gasparrini²¹,
 12 N. Gehrels^{22,34,35}, S. Germani^{13,14}, B. Giebels¹⁷, N. Giglietto^{15,16}, P. Giommi²¹, F. Giordano^{15,16},
 13 T. Glanzman³, G. Godfrey³, I. A. Grenier⁸, M.-H. Grondin^{30,31}, J. E. Grove¹, L. Guillemot^{36,30,31},
 14 S. Guiriec³⁷, A. K. Harding²², R. C. Hartman²², M. Hayashida³, E. Hays²², S. E. Healey³,
 15 D. Horan¹⁷, R. E. Hughes³⁸, M. S. Jackson^{39,6}, G. Jóhannesson³, A. S. Johnson³, W. N. Johnson¹,
 16 T. Kamae³, H. Katagiri³³, J. Kataoka⁴⁰, N. Kawai^{41,42}, M. Kerr¹⁸, J. Knödseder⁴³, M. Kuss⁷,
 17 J. Lande³, L. Latronico⁷, M. Lemoine-Goumard^{30,31}, F. Longo^{9,10}, F. Loparco^{15,16}, B. Lott^{30,31,*},
 18 M. N. Lovellette¹, P. Lubrano^{13,14}, G. M. Madejski³, A. Makeev^{1,25}, M. N. Mazziotta¹⁶,
 19 W. McConville^{22,35}, J. E. McEnery^{22,35}, C. Meurer^{27,6}, P. F. Michelson³, W. Mitthumsiri³,
 20 T. Mizuno³³, A. A. Moiseev^{23,35}, C. Monte^{15,16}, M. E. Monzani³, A. Morselli⁴⁴, I. V. Moskalenko³,
 21 S. Murgia³, P. L. Nolan³, J. P. Norris⁴⁵, E. Nuss²⁶, T. Ohsugi³³, N. Omodei⁷, E. Orlando⁴⁶,
 22 J. F. Ormes⁴⁵, D. Paneque³, J. H. Panetta³, D. Parent^{1,25,30,31}, V. Pelassa²⁶, M. Pepe^{13,14},
 23 M. Persic^{9,32}, M. Pesce-Rollins⁷, F. Piron²⁶, T. A. Porter⁴, S. Rainò^{15,16}, R. Rando^{11,12},
 24 M. Razzano⁷, A. Reimer^{47,3}, O. Reimer^{47,3}, T. Reposeur^{30,31}, S. Ritz^{4,4}, L. S. Rochester³,
 25 A. Y. Rodriguez¹⁹, R. W. Romani³, M. Roth¹⁸, F. Ryde^{39,6}, H. F.-W. Sadrozinski⁴, D. Sanchez¹⁷,
 26 A. Sander³⁸, P. M. Saz Parkinson⁴, J. D. Scargle⁴⁸, C. Sgrò⁷, E. J. Siskind⁴⁹, D. A. Smith^{30,31},
 27 P. D. Smith³⁸, G. Spandre⁷, P. Spinelli^{15,16}, M. S. Strickman¹, D. J. Suson⁵⁰, H. Tajima³,
 28 H. Takahashi³³, T. Takahashi⁵¹, T. Tanaka³, J. B. Thayer³, J. G. Thayer³, D. J. Thompson²²,
 29 L. Tibaldo^{11,12,8,52}, D. F. Torres^{53,19}, G. Tosti^{13,14}, A. Tramacere^{3,54}, Y. Uchiyama³, T. L. Usher³,
 30 V. Vasileiou^{23,24}, N. Vilchez⁴³, M. Villata⁵⁵, V. Vitale^{44,56}, A. P. Waite³, P. Wang³,
 31 B. L. Winer³⁸, K. S. Wood¹, T. Ylinen^{39,57,6}, M. Ziegler⁴

-
- ¹Space Science Division, Naval Research Laboratory, Washington, DC 20375, USA
- ²National Research Council Research Associate, National Academy of Sciences, Washington, DC 20001, USA
- ³W. W. Hansen Experimental Physics Laboratory, Kavli Institute for Particle Astrophysics and Cosmology, Department of Physics and SLAC National Accelerator Laboratory, Stanford University, Stanford, CA 94305, USA
- ⁴Santa Cruz Institute for Particle Physics, Department of Physics and Department of Astronomy and Astrophysics, University of California at Santa Cruz, Santa Cruz, CA 95064, USA
- ⁵Department of Astronomy, Stockholm University, SE-106 91 Stockholm, Sweden
- ⁶The Oskar Klein Centre for Cosmoparticle Physics, AlbaNova, SE-106 91 Stockholm, Sweden
- ⁷Istituto Nazionale di Fisica Nucleare, Sezione di Pisa, I-56127 Pisa, Italy
- ⁸Laboratoire AIM, CEA-IRFU/CNRS/Université Paris Diderot, Service d’Astrophysique, CEA Saclay, 91191 Gif sur Yvette, France
- ⁹Istituto Nazionale di Fisica Nucleare, Sezione di Trieste, I-34127 Trieste, Italy
- ¹⁰Dipartimento di Fisica, Università di Trieste, I-34127 Trieste, Italy
- ¹¹Istituto Nazionale di Fisica Nucleare, Sezione di Padova, I-35131 Padova, Italy
- ¹²Dipartimento di Fisica “G. Galilei”, Università di Padova, I-35131 Padova, Italy
- ¹³Istituto Nazionale di Fisica Nucleare, Sezione di Perugia, I-06123 Perugia, Italy
- ¹⁴Dipartimento di Fisica, Università degli Studi di Perugia, I-06123 Perugia, Italy
- ¹⁵Dipartimento di Fisica “M. Merlin” dell’Università e del Politecnico di Bari, I-70126 Bari, Italy
- ¹⁶Istituto Nazionale di Fisica Nucleare, Sezione di Bari, 70126 Bari, Italy
- ¹⁷Laboratoire Leprince-Ringuet, École polytechnique, CNRS/IN2P3, Palaiseau, France
- ¹⁸Department of Physics, University of Washington, Seattle, WA 98195-1560, USA
- ¹⁹Institut de Ciències de l’Espai (IEEC-CSIC), Campus UAB, 08193 Barcelona, Spain
- ²⁰INAF-Istituto di Astrofisica Spaziale e Fisica Cosmica, I-20133 Milano, Italy
- ²¹Agenzia Spaziale Italiana (ASI) Science Data Center, I-00044 Frascati (Roma), Italy
- ²²NASA Goddard Space Flight Center, Greenbelt, MD 20771, USA
- ²³Center for Research and Exploration in Space Science and Technology (CRESST) and NASA Goddard Space Flight Center, Greenbelt, MD 20771, USA
- ²⁴Department of Physics and Center for Space Sciences and Technology, University of Maryland Baltimore County, Baltimore, MD 21250, USA
- ²⁵George Mason University, Fairfax, VA 22030, USA
- ²⁶Laboratoire de Physique Théorique et Astroparticules, Université Montpellier 2, CNRS/IN2P3, Montpellier, France
- ²⁷Department of Physics, Stockholm University, AlbaNova, SE-106 91 Stockholm, Sweden
- ²⁸Royal Swedish Academy of Sciences Research Fellow, funded by a grant from the K. A. Wallenberg Foundation
- ²⁹Dipartimento di Fisica, Università di Udine and Istituto Nazionale di Fisica Nucleare, Sezione di Trieste, Gruppo

Collegato di Udine, I-33100 Udine, Italy

³⁰CNRS/IN2P3, Centre d'Études Nucléaires Bordeaux Gradignan, UMR 5797, Gradignan, 33175, France

³¹Université de Bordeaux, Centre d'Études Nucléaires Bordeaux Gradignan, UMR 5797, Gradignan, 33175, France

³²Osservatorio Astronomico di Trieste, Istituto Nazionale di Astrofisica, I-34143 Trieste, Italy

³³Department of Physical Sciences, Hiroshima University, Higashi-Hiroshima, Hiroshima 739-8526, Japan

³⁴Department of Astronomy and Astrophysics, Pennsylvania State University, University Park, PA 16802, USA

³⁵Department of Physics and Department of Astronomy, University of Maryland, College Park, MD 20742, USA

³⁶Max-Planck-Institut für Radioastronomie, Auf dem Hügel 69, 53121 Bonn, Germany

³⁷Center for Space Plasma and Aeronomic Research (CSPAR), University of Alabama in Huntsville, Huntsville, AL 35899, USA

³⁸Department of Physics, Center for Cosmology and Astro-Particle Physics, The Ohio State University, Columbus, OH 43210, USA

³⁹Department of Physics, Royal Institute of Technology (KTH), AlbaNova, SE-106 91 Stockholm, Sweden

⁴⁰Research Institute for Science and Engineering, Waseda University, 3-4-1, Okubo, Shinjuku, Tokyo, 169-8555 Japan

⁴¹Department of Physics, Tokyo Institute of Technology, Meguro City, Tokyo 152-8551, Japan

⁴²Cosmic Radiation Laboratory, Institute of Physical and Chemical Research (RIKEN), Wako, Saitama 351-0198, Japan

⁴³Centre d'Étude Spatiale des Rayonnements, CNRS/UPS, BP 44346, F-30128 Toulouse Cedex 4, France

⁴⁴Istituto Nazionale di Fisica Nucleare, Sezione di Roma "Tor Vergata", I-00133 Roma, Italy

⁴⁵Department of Physics and Astronomy, University of Denver, Denver, CO 80208, USA

⁴⁶Max-Planck Institut für extraterrestrische Physik, 85748 Garching, Germany

⁴⁷Institut für Astro- und Teilchenphysik and Institut für Theoretische Physik, Leopold-Franzens-Universität Innsbruck, A-6020 Innsbruck, Austria

⁴⁸Space Sciences Division, NASA Ames Research Center, Moffett Field, CA 94035-1000, USA

⁴⁹NYCB Real-Time Computing Inc., Lattingtown, NY 11560-1025, USA

⁵⁰Department of Chemistry and Physics, Purdue University Calumet, Hammond, IN 46323-2094, USA

⁵¹Institute of Space and Astronautical Science, JAXA, 3-1-1 Yoshinodai, Sagami-hara, Kanagawa 229-8510, Japan

⁵²Partially supported by the International Doctorate on Astroparticle Physics (IDAPP) program

⁵³Institució Catalana de Recerca i Estudis Avançats (ICREA), Barcelona, Spain

⁵⁴Consorzio Interuniversitario per la Fisica Spaziale (CIFS), I-10133 Torino, Italy

⁵⁵INAF, Osservatorio Astronomico di Torino, I-10025 Pino Torinese (TO), Italy

⁵⁶Dipartimento di Fisica, Università di Roma "Tor Vergata", I-00133 Roma, Italy

⁵⁷School of Pure and Applied Natural Sciences, University of Kalmar, SE-391 82 Kalmar, Sweden

* Corresponding author. Email: lott@cenbg.in2p3.fr

ABSTRACT

The gamma-ray energy spectra of bright blazars of the LAT Bright AGN Sample (LBAS) are investigated using *Fermi*-LAT data. Spectral properties (hardness, curvature and variability) established using a data set accumulated over 6 months of operation are presented and discussed for different blazar classes and subclasses: Flat Spectrum Radio Quasars (FSRQs), Low-synchrotron peaked BLLacs (LSP-BLLacs), Intermediate-synchrotron peaked BLLacs (ISP-BLLacs) and High-synchrotron peaked BLLacs (HSP-BLLacs). The distribution of photon index (Γ , obtained from a power-law fit above 100 MeV) is found to correlate strongly with blazar subclass. The change in spectral index from that averaged over the six month observing period is $< 0.2-0.3$ when the flux varies by about an order of magnitude, with a tendency toward harder spectra when the flux is brighter for FSRQs and LSP-BLLacs. A strong departure from a single power-law spectrum appears to be a common feature for FSRQs. This feature is also present for some high-luminosity LSP-BLLacs, and a small number of ISP-BLLacs. It is absent in all LBAS HSP-BLLacs. For 3C 454.3 and AO 0235+164, the two brightest FSRQ source and LSP-BLLac source respectively, a broken power law gives the most acceptable of power law, broken power law, and curved forms. The consequences of these findings are discussed.

Subject headings: gamma rays: observations — galaxies: active — galaxies: jets — BL Lacertae objects: general

1. Introduction

Launched into a low-Earth orbit on June 11, 2008, the *Fermi Gamma-Ray Space Telescope* continues providing excellent gamma-ray data for celestial sources. With significant improvement of sensitivity and bandpass over its predecessors (Atwood et al. 2009), the main instrument on *Fermi* - the Large Area Telescope, or LAT - enables detailed studies of time-resolved broad-band gamma-ray spectra of a broad range of sources, including active galaxies. As discovered by EGRET on the Compton Observatory (Hartman et al. 1992; Fichtel et al. 1994), active galactic nuclei (AGN) showing strong gamma-ray emission are associated with relativistic jets, whose presence was independently inferred from morphological and variability studies in other bands. The spectra of such objects in all observable bands are well-described by broad power-law or curved distributions, indicating non-thermal emission mechanisms (Böttcher 2007). Very generally, the overall broad-band spectral distributions of such jet-dominated AGN, often called blazars have a two-humped shape, with the low energy (IR-UV) hump attributed to synchrotron emission of energetic electrons radiating in magnetic field and the high energy hump due to inverse Compton scattering by the same electrons (Ghisellini 1989; Dermer & Schlickeiser 1993; Sikora et al. 1994).

51 The first list of such AGN detected by the *Fermi*-LAT, the LAT Bright AGN Sample (LBAS)
 52 (Abdo et al. 2009e) includes bright, high-galactic latitude ($|b| > 10^\circ$) AGNs detected by the Fermi-
 53 LAT with high significance (Test Statistic $TS > 100$) during the first three months of scientific
 54 operation. This sample comprises 58 Flat Spectrum Radio Quasars (FSRQs), 42 BLLac-type ob-
 55 jects (BLLacs), two radio galaxies and four quasars of unknown type. This somewhat conventional
 56 classification was based on the observed optical emission line equivalent widths and the Ca II break
 57 ratio (e.g., Marcha et al. 1996). Following the models used to describe the gamma-ray spectra ob-
 58 tained with previous gamma-ray observatories (e.g., Mattox et al. 1996), the early analysis reported
 59 in (Abdo et al. 2009e) was carried out by fitting the gamma-ray spectra at energies above 200 MeV
 60 using a simple power law (PL) model. This analysis revealed a fairly distinct spectral separation
 61 between FSRQs and BLLacs, with FSRQs having significantly softer spectra. The boundary pho-
 62 ton index between the two classes was found to be $\Gamma \simeq 2.2$. It has been suggested (Ghisellini et al.
 63 2009) that this separation results from different radiation cooling suffered by the electrons due to
 64 distinct accretion regimes in the two blazar classes.

65 While adopting such a simple spectral model was sufficient to investigate the source spectral
 66 hardness distribution, a PL model was clearly not the most appropriate choice for some bright
 67 sources which exhibited evident breaks or curvatures in their spectra. The departure of the func-
 68 tional form from a PL was investigated in some detail for the bright quasar 3C 454.3 (Abdo et al.
 69 2009d), which underwent strong activity in the summer of 2008. The change of photon index $\Delta\Gamma$
 70 was observed to be 1.2 ± 0.2 , i.e. greater than the value of 0.5 expected from incomplete cooling of
 71 the emitting electrons. The observed break around 2.2 GeV was ascribed to mirroring a similar
 72 feature in the underlying emitting electron energy distribution; the Klein-Nishina effect was not
 73 ruled out, though the importance of photon-photon pair production requires the gamma-ray emis-
 74 sion region to be close to the supermassive black hole. Clearly, understanding the details of the
 75 spectral break is important for understanding the structure and location of the dissipation region
 76 of jets in active galaxies.

77 The data first obtained with the EGRET instrument, now refined with Fermi, imply that the
 78 high Galactic latitude sky emits quasi-diffuse, uniform gamma-ray background (Sreekumar et al.
 79 1998; Strong et al. 2004a; Abdo et al. 2009b). Its isotropy points to its extragalactic nature after
 80 subtraction of a quasi-isotropic gamma-ray emission component from cosmic ray electrons in an
 81 extended galactic halo. Most models account for at least a part of this background as originat-
 82 ing from a large number of unresolved point sources, presumably jet-dominated AGN. Here, the
 83 comparison of spectral properties of various classes of AGN, integrated over their space density
 84 and luminosity, against the integral measurement of the unresolved component should provide ad-
 85 ditional clues regarding their contribution to the extragalactic diffuse background: can they make
 86 up the entire background, is another class of sources, e. g. star-forming galaxies (Fields et al.
 87 2008) or is an additional truly diffuse component required? The issue is further complicated by
 88 the apparently different spectral forms of the luminous AGN associated with quasars as compared
 89 to the lineless BL Lac objects, as already hinted in Abdo et al. (2009e). It is thus important to

90 determine whether the spectral feature seen in 3C 454.3 is common in all blazars and also whether
 91 it is connected to other blazar properties.

92 Here we report on the detailed spectral analysis of bright LBAS sources using data accumulated
 93 over the first 6 months of the *Fermi*-LAT all-sky survey. In Section 2, we present the observations
 94 with the *Fermi*-LAT; Section 3 briefly discusses the classification scheme used in this paper. Section
 95 4 contains the results regarding the photon index and observed deviations from a pure PL. The
 96 results and their consequences are discussed in Section 5.

97 2. Observations with the Large Area Telescope

98 The *Fermi*-LAT is a pair-conversion gamma-ray telescope sensitive to photon energies greater
 99 than 20 MeV. It is made of a tracker (composed of two sections, front and back, with different
 100 localization capabilities), a calorimeter, and an anticoincidence system to reject the charged-particle
 101 background. The LAT has a large peak effective area ($\sim 8000 \text{ cm}^2$ for 1 GeV on-axis photons in the
 102 event class “diffuse” considered here), viewing $\approx 2.4 \text{ sr}$ of the full sky with an angular resolution
 103 (68% containment angle) better than $\approx 1^\circ$ at $E = 1 \text{ GeV}$ (Atwood et al. 2009).

104 The data were collected from 4 Aug. 2008 to 1 Feb. 2009 in survey mode. To minimize
 105 systematics, only photons with energies greater than 100 MeV were considered in this analysis. In
 106 order to avoid contamination from Earth limb gamma-rays, a selection on the zenith angle, $< 105^\circ$,
 107 was applied. The exposure was constant within 20% for all sources and amounted to about 1.5×10^6
 108 m^2s at 1 GeV.

109 This analysis was performed with the standard analysis tool *glike*, part of the Fermi-LAT
 110 ScienceTools software package (version v9r12). The first set of instrument response functions (IRFs)
 111 tuned with the flight data, P6_V3_DIFFUSE, was used. In contrast to the preflight IRFs, these
 112 IRFs take into account corrections for pile-up effects. This correction being higher for lower energy
 113 photons, the measured photon index of a given source is about 0.1 higher (i.e. the spectrum is softer)
 114 with this IRF set as compared to the P6_V1_DIFFUSE one used previously in Abdo et al. (2009e).
 115 Photons were selected in circular regions of interest (ROI), 7° in radius, centered at the positions
 116 of the sources of interest. The isotropic background (the sum of residual instrumental background
 117 and extragalactic diffuse gamma-ray background) was modeled with a simple power-law. The
 118 GALPROP model (Strong et al. 2004a,b), version “gll_iem_v01.fit”, was used for the galactic diffuse
 119 emission, with both flux and spectral photon index left free in the fit. All point sources with $\text{TS} > 25$
 120 in the 6-month source list, lying within the ROI and a surrounding 5° -wide annulus, were modeled
 121 in the fit with single power-law distributions. Different analyses were performed by fitting the
 122 spectra with various models over the whole energy range covered by the LAT above 100 MeV,
 123 or with a PL model over equispaced logarithmic energy bins (where the spectral index was kept
 124 constant and equal to the value fitted over the whole range). In the case of fits with broken
 125 power law (BPL) models, the break energy (E_{Break}) bounding the ranges where different photon

126 indices (Γ_1 and Γ_2) apply, could not be obtained directly from the fit for most sources because of
 127 convergence problem due the non-smooth character of the BPL function at the break energy. It was
 128 computed from a loglikelihood profile fitting procedure, with statistical uncertainties corresponding
 129 to a difference of $-2\Delta L=1$ in the loglikelihood (L) with respect to its minimum. We refer the reader
 130 to ref. (D’Agostini 2004) regarding limitations with the use of asymmetric uncertainties.

131 The estimated systematic uncertainty on the flux is 10% at 100 MeV, 5% at 500 MeV and
 132 20% at 10 GeV. The energy resolution is better than 10% over the range of measured E_{Break} .

133 3. Classification

134 We employ the conventional definition of BL Lac objects outlined in Stocke et al. (1991);
 135 Urry & Padovani (1995); Marcha et al. (1996) in which the equivalent width of the strongest opti-
 136 cal emission line is $< 5 \text{ \AA}$ and the optical spectrum shows a Ca II H/K break ratio $C < 0.4$. BLLac
 137 sources were assigned to different subclasses (LSP-BLLacs, ISP-BLLacs and HSP-BLLacs standing
 138 for Low-, Intermediate-, and High-synchrotron peaked BLLacs respectively) according to the posi-
 139 tion of their synchrotron peak, established from radio, optical, UV and X-ray data: $\nu_{peak} < 10^{14}$
 140 Hz for LSP-BLLacs, $10^{14}\text{Hz} < \nu_{peak} < 10^{15}\text{Hz}$ for ISP-BLLacs and $\nu_{peak} > 10^{15}\text{Hz}$ for HSP-BLLacs
 141 (Abdo et al. 2009f). Contemporaneous Swift data were used for a subset of 46 LBAS sources and
 142 archival ones for the others, as described in Abdo et al. (2009f).

143 4. Results

144 4.1. Photon index distributions

145 Although some spectra display significant curvatures, the photon index obtained by fitting
 146 single power-law models over the whole LAT energy range provides a convenient means to study
 147 the spectral hardness. Fig. 1 displays the distributions of the resulting photon index for the
 148 four different subclasses. The remarkable separation between FSRQs and BLLacs already found
 149 in Abdo et al. (2009e) is of course still observed for spectra averaged over a 6-month (instead
 150 of 3-month) time span. Likewise, different BLLac subclasses are associated with distinct photon
 151 index distributions in the LAT range. The distributions have (mean, rms)=(2.46, 0.18) for FSRQs,
 152 (2.21, 0.16) for LSP-BLLacs, (2.13, 0.17) for ISP-BLLacs and (1.86, 0.17) for HSP-BLLacs. For
 153 comparison, the distributions given in Abdo et al. (2009e) had (mean, rms)= (2.40, 0.17), (1.99,
 154 0.22) for FSRQs and BL Lacs respectively. It must be kept in mind that the 6-month distributions
 155 have been obtained with an improved (more realistic) IRF set leading to a softer measured spectrum
 156 (Γ higher by $\simeq 0.1$ unit). Interestingly, the largest difference (increase) in photon index between the
 157 3-month and the 6-month data set is obtained for BL Lacertae (from $\Gamma=2.24\pm 0.12$ to $\Gamma=2.54\pm 0.07$),
 158 a BLLac intermittently exhibiting broad emission lines characteristic of FSRQs (Vermeulen et al.

159 1995). It would be interesting to investigate the correlation of this spectral evolution with properties
 160 in other bands.

161 The distributions in Fig. 1 are remarkably narrow, with rms =0.16-0.18, i. e. comparable to
 162 the index statistical uncertainties for the faintest LBAS sources. Note that the overlap between
 163 LSP-BLLac and FSRQ photon index distributions is small (LSP-BLLacs being harder), although
 164 both have similar positions of their synchrotron peaks. The gamma-ray photon index is thus a
 165 distinctive property of a blazar subclass. The low dispersion observed within a subclass strongly
 166 supports the idea that a very limited number of physical parameters (possibly only one), drive the
 167 spectrum shape in the GeV energy range. It can also be connected to distinct dominant emission
 168 mechanisms for the different classes, External Compton for the low-energy peaked sources and
 169 Synchrotron Self Compton for the high-energy peaked ones, as discussed in Abdo et al. (2009f).

170 One must keep in mind that the LBAS sample, being significance limited (TS>100 after 3
 171 months of LAT operation) has an intrinsic bias such that faint sources can more easily be detected
 172 if they are hard. This situation is illustrated in Fig. 2 (similar to Fig. 7 in Abdo et al. 2009e), where
 173 the 6-month average photon index flux is plotted vs the corresponding flux for the four subclasses
 174 along with the approximate LBAS flux limit (for the first 3 months of operation). From this figure,
 175 the source subclass that appears potentially the most affected by this bias is that of HSP-BLLacs,
 176 which are substantially fainter than the other sources. However, as pointed out in Abdo et al.
 177 (2009f), more than 60% of known radio-loud HSP-BLLacs are included in the LBAS sample, so the
 178 measured photon index distribution is probably still representative of the full population.

179 4.2. Photon index variability

180 Given the narrowness of the photon index distribution for a given class, the photon index
 181 would not be expected to vary wildly over time for a given source. Two examples of weekly flux
 182 and photon index light curves are shown in Fig. 3 for the brightest FSRQ (3C 454.3) and LSP-
 183 BLLac (AO 0235+164) in the LBAS. The average photon index is shown as a dashed line in the
 184 corresponding panels. Although flux variations are large (flux variations by a factor >7) for both
 185 sources, the range of photon index values is only about 0.3 wide if one allows for a one-sigma
 186 dispersion. The insets in Fig. 3 display the photon index resulting from an analysis where photons
 187 were sorted in five bins in weekly flux, plotted vs the weekly flux. A weak “harder when brighter”
 188 effect can be seen for both sources.

189 To test the constancy of the photon index, the weekly photon indices were fitted with a constant
 190 model and the corresponding fractional excess variance (Vaughan et al. 2003) was calculated for
 191 the different LBAS sources, keeping only time periods where the sources were detected with a
 192 significance larger than 3σ . Fig. 4 top displays the distributions of normalized χ^2 values obtained
 193 for FSRQs (red), BLLacs (blue) and all sources (black). The means of these distributions are close
 194 to 1, as expected for a constant photon index, with no significant differences between FSRQs and

195 BLLacs. For illustration, the normalized χ^2 distribution with 20 degrees of freedom (corresponding
 196 to an average source) expected in the case of a constant photon index is plotted as well. The source
 197 associated with a normalized χ^2 of 3.5 is PKS 1502+106 for which a clear indication of “harder
 198 when brighter” effect has been observed during a bright flare (Abdo et al. 2009a). Fig. 4 bottom
 199 shows the distributions of fractional excess variance for FSRQs and BLLacs. The means of the
 200 distributions are compatible with 0 (within 1σ); the same applies for all three BLLac subclasses.
 201 The widths of these distributions are in good agreement with the average statistical uncertainties
 202 (estimated from Eq. 11 in Vaughan et al. 2003), i.e. 8×10^{-3} and 1.5×10^{-2} for FSRQs and BLLacs
 203 respectively. Inspection of distributions of Pearson coefficients of the weekly flux vs photon index
 204 correlation does not reveal any strong trend for any subclass. The average variation of weekly
 205 photon index is plotted vs the relative flux (normalized to the average flux) in Fig. 5 for the
 206 different blazar subclasses. The data from the eight brightest representatives of each subclass have
 207 been considered¹. A weak “harder when brighter” effect is apparent in FSRQs, LSP-BLLacs and
 208 ISP-BLLacs, whereas no significant effect is present for HSP-BLLacs².

209 These observations, aimed at determining the gross spectral features of a source ensemble, do
 210 not exclude fine spectral evolutions over short periods of time, e.g. regarding particular episodes
 211 of flaring activity, or for particular sources. They do, however, demonstrate that the photon index
 212 in the GeV range changes little with time and within a blazar subclass.

213 4.3. Spectra of brightest sources

214 In this section we present the spectra obtained for the eight brightest representatives of the
 215 four subclasses, FSRQs (Fig. 6), LSP-BLLacs (Fig. 7), ISP-BLLacs (Fig. 8), and HSP-BLLacs
 216 (Fig. 9), ordered according to decreasing average flux. Upper limits are shown for bins associated
 217 with a TS lower than 9 (significance lower than 3σ) or with a number of source photons (predicted
 218 by the model) lower than 3. The brightest FSRQ, 3C 454.3 with an average flux ($E>100$ MeV) of
 219 2×10^{-6} ph cm⁻²s⁻¹, exhibits a pronounced break around 2 GeV, as reported in Abdo et al. (2009d).
 220 Indications for breaks between 1 and 10 GeV are observed for essentially all of these FSRQ sources.
 221 This behavior is confirmed by comparing (Fig. 11) the flux ($E>2$ GeV) extrapolated from the
 222 spectral distribution in the range $100\text{ MeV} < E < 2\text{ GeV}$, fitted with a power-law function, with the
 223 actual measured flux (obtained via a power-law fit in the $E>2$ GeV energy range). For all sources
 224 considered, the measured flux is lower than the extrapolated flux by more than 30%. The spectral
 225 properties of these sources are summarized in Table 1, which gives also the difference in loglikelihood
 226 between the BPL and PL fits, the break energy in the source rest frame, $E'_{Break}=E_{Break}\times(1+z)$,
 227 and the source gamma-ray luminosity (computed as in Ghisellini et al. 2009). E'_{Break} lies between

¹A condition on the significance $> 1\sigma$, i.e. less restrictive than above, has been imposed in this analysis to minimize the effect of the instrumental bias against soft and faint states illustrated in Fig. 2.

²The weak tendency toward softer spectra at high flux in HSP-BLLacs does not appear to be significant.

228 1.6 and 10 GeV for all sources listed in Table 1. No significant correlation is found between E'_{Break}
 229 and the gamma-ray luminosity (Fig. 10).

230 The presence of a break is also clear for two of the brightest LSP-BLLacs (associated with
 231 the highest luminosities, Table 2) in the LBAS sample, AO 0235+164 and PKS 0537-441 (Fig. 7),
 232 while it is less apparent for the fainter ones. From the inspection of these spectra, it can already
 233 be noted that the onset of the break, when present, seems to be located at higher energy than in
 234 the case of FSRQs while E'_{Break} lies in about the same range.

235 Some ISP-BLLacs (Fig. 8) present clear signs of breaks (e.g. S5 0716+71, S2 0109+22), while
 236 the rest, having in some cases very hard spectra, are compatible with power-law distributions up to
 237 several tens of GeV. Finally, no bright HSP-BLLac (Fig. 9) shows any evidence for a break in the
 238 LAT energy range. This simple observation, which could be naively expected for sources many of
 239 which are detected at TeV energies, definitely rules out an instrumental effect as the origin of the
 240 break found for lower-energy peaked sources. The indication for a moderate break in PKS 2155-304
 241 (Aharonian et al. 2009) observed over a short time period (11 days) does not persist over a 6-month
 242 integration time.

243 For a small number of sources exhibiting the break, a few photons compatible with the source
 244 location are detected at high energy, at variance with the decreasing trend. Most of these have
 245 been cut off by the condition on the minimum number of photons per bin (3). More statistics
 246 will be required to determine whether these photons do arise from these sources or just represent
 247 background fluctuations.

248 Fig. 11 illustrates the general trend for the four subclasses. The trend observed in the presence
 249 of a spectral break (or curvature) parallels that observed in the photon index for the four different
 250 classes.

251 4.4. Spectra of special sources

252 For 19 of the 22 brightest LBAS FSRQs, a likelihood ratio test (LRT, Mattox et al. 1996)
 253 rejects the hypothesis that the spectrum is a PL (null hypothesis) against the one that the spectrum
 254 is a BPL, at a confidence level greater than 97%. The four top panels of Fig. 12 show spectra of
 255 representative sources where the break is clear. The spectral properties of these sources (PL and
 256 BPL fit results, difference in logLikelihood between the two fits) are reported in Table 1 as well.
 257 The two bottom left panels correspond to two of the three sources having the confidence level less
 258 than 97% (the other being PKS 2022-07, whose spectrum is given in Fig. 6). For these two sources,
 259 a break located around 10 GeV cannot be excluded.

260 The last two panels of Fig. 12 present the energy spectra of sources of particular interest,
 261 Mrk 501 and 1ES 0502+675. Mrk 501, the archetypal example of an extreme HSP-BLLac, is hard
 262 ($\Gamma=1.75\pm 0.06$) and does not exhibit any sign of curvature, in keeping with the behavior of the

263 other HSP-BLLacs. The other one corresponds to 1ES 0502+675, an HSP-BLLac which exhibits
 264 an unusual concave energy spectrum ($\Gamma_1=2.68\pm0.18, \Gamma_2=1.47\pm0.10, E_{break}=1.4\pm0.6$ GeV). The
 265 LRT indicates that a BPL model is favored against a PL with a significance level of 2×10^{-4} . The
 266 very hard spectrum above 1.4 GeV would make this source a prime target for TeV observations
 267 although the redshift is fairly large (0.416).

268 4.5. Detailed analysis of 3C 454.3 and AO 0235+164 energy spectra

269 The data accumulated over 6 months enable us to discriminate between different spectral
 270 models for the two brightest sources with spectra exhibiting strong departure from a pure PL,
 271 namely 3C 454.3 and AO 0235+164. Fig. 13 shows the results of fits with different models: PL
 272 (thin lines), BPL(thick solid) and log-parabola (dashed) are compared with the data. Surpris-
 273 ingly, a broken power-law model is favored as the best fit for both sources. Despite the good
 274 statistics, no curvature is apparent in the energy range below the break. The fitted parameters
 275 are: $F[E>100 \text{ MeV}]=1.97\pm0.03\times10^{-6} \text{ ph cm}^{-2}\text{s}^{-1}$, $\Gamma_1=2.39\pm0.02$, $\Gamma_2=3.42\pm0.11$, $E_{break}=2.5\pm0.3$
 276 GeV for 3C 454.3 and $F[E>100 \text{ MeV}]=0.60\pm0.02\times10^{-6} \text{ ph cm}^{-2}\text{s}^{-1}$, $\Gamma_1=2.05\pm0.02$, $\Gamma_2=2.95\pm0.16$,
 277 $E_{break}=4.5^{+1.5}_{-1.0}$ GeV for AO 0235+164. While the break energy is somewhat larger for AO 0235+164
 278 than for 3C 454.3, the photon index change ($\Gamma_2 - \Gamma_1$) is about the same (0.90 ± 0.16 vs 1.03 ± 0.11).
 279 The similarity of the break feature for two sources belonging to different subclasses, FSRQ and LSP-
 280 BLLac, with different line strengths, seems to rule out any absorption effect in the LSP-BLLacs.

281 4.6. Apparent curvature due to varying spectral hardness

282 An energy spectrum with time varying hardness may exhibit an apparent curvature when in-
 283 tegrated over an extended period of time. To assess the magnitude of this effect, both analytical
 284 estimates and simulations assuming pure power-law distributions with flux and photon index cor-
 285 responding to those actually measured over weekly time bins have been performed. Fig. 3 shows
 286 the 3C 454.3 and AO 0235+164 weekly light curves and corresponding photon index. With these
 287 input data, the calculated spectra (assuming constant exposure) are not found to exhibit significant
 288 curvatures (Fig. 14). Fig. 15 compares the simulated photon count distribution obtained within
 289 the 90% containment radius around the source (blue) with the data (black). The effect of spectral
 290 hardness varying with time clearly cannot alone account for the observed features.

291 5. Discussion

292 The trend in the observed gamma-ray photon index reported here confirms that reported earlier
 293 using three months of data: FSRQs, with a gamma-ray photon index greater than 2, are softer than
 294 BLLacs, indicating that the peak of the high-energy component in FSRQS is always lower than

295 100 MeV. For BLLacs, the gamma-ray photon index correlates with the different BLLac subclasses,
 296 which themselves are defined by the position of the synchrotron peak. The measured photon index
 297 shifts from $\Gamma > 2$ to $\Gamma < 2$, indicating that the peak energy of the high-energy component of the
 298 spectral energy distribution (SED) sweeps across the Fermi energy range from LSP-BLLacs to
 299 HSP-BLLacs.

300 The photon index being related to the shape of the emitting electron energy distributions,
 301 different regions of the electron distributions (from the high- to the low-energy ends for FSRQs/LSP-
 302 BLLacs and HSP-BLLacs respectively) are probed in the LAT range. One would thus expect
 303 different spectral variability patterns in the LAT energy range for different blazar classes.

304 Using weekly light curves obtained over the first 6 months of LAT operation, this expectation
 305 does not seem to be corroborated by the data. The gamma-ray photon index appears remarkably
 306 stable with time, irrespective of the blazar class. This feature is in line with the observed narrowness
 307 of the index distribution for a class: a strongly varying photon index for a source would inevitably
 308 lead to a broad class distribution as different sources would be “caught” in different states. This
 309 apparent constancy of the photon index for all blazar classes may appear surprising, since for
 310 different classes, different electron energies (potentially associated with different cooling timescales,
 311 t_{cool}) emit gamma-rays in the LAT energy range. However, estimates of the cooling time show that
 312 within one week, all pairs with Lorentz factors $\gamma > 5/\delta_{10}u'$ have cooled down (where δ_{10} is the
 313 Doppler factor $\delta/(1+z)$ divided by 10, and u' is the jet frame energy density in erg cm^{-3} of the
 314 ambient magnetic field, or photon field provided scattering occurs in the Thomson regime). For
 315 sufficiently large u' the LAT energy range falls in the complete cooling regime. Spectral hysteresis
 316 may then be expected on time scales shorter than weekly if the duration of electron injection is
 317 sufficiently limited $\ll t_{\text{cool}}$. Flux variations on weekly time scales may then reflect a varying injected
 318 energy content into the emission region from one week to another. Alternatively, continuous particle
 319 injection on at least weeks time scale could stabilize the spectral index. In the case of lower u' ,
 320 constant spectral indices can still be expected during flux variations in the LAT energy range if
 321 continuous particle injection is maintained for a time range significantly longer than the cooling
 322 time of the gamma-ray emitting particles (e.g. Kirk & Mastichiadis 1999). Flux changes then
 323 constrain the duration of particle injection. As more data are accumulated, possible exceptions to
 324 the observed index stability may appear. However, we can safely claim that a very soft spectrum
 325 for an HSP-BLLac, like that reported from EGRET for PKS 2155-304, $\Gamma=2.35$ (Hartman et al.
 326 1999), or a very hard one for a FSRQ, like the one reported from AGILE for 3C 454.3, $\Gamma=1.7$
 327 (Vercellone et al. 2009), represent very rare occurrences.

328 All blazar spectra measured by EGRET were represented with pure PL. Thanks to its improved
 329 sensitivity, Fermi has revealed that the spectra of some low-energy peaked blazars display strong
 330 departure from a pure-PL behavior, with a BPL function as the best model. This feature being
 331 present for essentially all FSRQs where it can be detected with sufficient significance, it is likely to be
 332 a general character of this class. The three brightest LSP-BLLacs, in which this effect is also clearly
 333 seen, have higher luminosity ($L_{\gamma} > 10^{47} \text{ erg s}^{-1}$) than the rest of the LBAS LSP-BLLacs. Two of

334 them are known to exhibit broad emission lines in low emission states, so could be FSRQs whose
 335 lines are hidden by non-thermal emission in active states. As discussed in Abdo et al. (2009d), the
 336 difference in photon index for most sources is significantly larger than 0.5 expected for an incomplete
 337 cooling effect. An absorption effect seems to be ruled out as well, since to produce a break in the 1-
 338 10 GeV, the photon field should have an energy peaking in the 0.05-0.5 KeV range, which excludes
 339 the broad-line region peaking in the UV. This feature most likely reflects the energy distribution
 340 of the emitting electrons. For the low-energy peaked sources where it is seen, Γ is greater than
 341 2, i.e. the LAT range corresponds to “the falling edge” of the IC hump, where the highest energy
 342 electrons contribute. This feature could indicate a cutoff in that distribution, possibly related to
 343 limitations in the acceleration process (e.g. Drury 1991; Webb et al. 1984). Comparison of the
 344 maximum electron energies determined by the SED for PKS 2155-304, an HSP-BLLac where a
 345 one-zone synchrotron/SSC model was applied to derive the magnetic field and Doppler factor,
 346 showed that such an interpretation requires that the acceleration rate be approximately 3 orders
 347 of magnitude smaller than the maximum acceleration rate determined by the Larmor timescale
 348 (Finke et al. 2008). A Klein-Nishina break, expected in the context of a dominating External
 349 Compton emission process where the electrons upscatter BLR photons, is predicted to set in around
 350 $\frac{15\delta}{\Gamma(1+z)}$ GeV, where Γ is the blob bulk Lorentz factor (Ghisellini & Tavecchio 2009), i. e. significantly
 351 higher than the energies found here.

352 Irrespective of its origin, this feature, common for FSRQs and some LSP-BLLacs, has impor-
 353 tant practical consequences. First, it surely complicates the assessment of EBL attenuation effects
 354 using FSRQs and LSP-BLLacs, as fewer photons are detected in the >10 GeV energy range. Sec-
 355 ond, as the low-energy peaked blazars are likely to represent the bulk of the blazar population, this
 356 break must manifest itself in (and be considered when evaluating) the contribution of unresolved
 357 blazars to the extragalactic diffuse γ -ray background. Finally, this effect must be considered when
 358 estimating the detectability of a source in the TeV range.

359 The concave shaped SED measured for the X-ray selected object 1ES 0502+675 ($z=0.416$)
 360 opens interesting questions. It could potentially be a spurious feature resulting from the spatial
 361 confusion of a hard source with a soft one. No evidence for a second source has been found using
 362 the *gttstmap* tool of the standard ScienceTools package. The closest CRATES source is 1.5° away.
 363 If confirmed, this peculiar spectral shape indicates either two components (e.g. Synchrotron-Self
 364 Compton and External Compton in the context of leptonic models) in the high-energy SED (how-
 365 ever not expected in HSP-BLLacs in the framework of one-zone leptonic models), or the turnover
 366 from the synchrotron to the high-energy component, although the contemporaneous spectral en-
 367 ergy distributions (Abdo et al. 2009f) obtained during that period does not seem to support that
 368 interpretation. This object should be a prime target for TeV instruments, opening interesting
 369 perspectives for studies on EBL absorption at TeV energies given its redshift.

370 A similar behavior, although less significant, has also been found for 1ES 1959+650 (Fig. 8)
 371 and PG 1246+586, which is not included in the LBAS sample but is present in the LAT Bright

372 Source List³ (Abdo et al. 2009c). The spectra of other sources (e.g. W Comae) exhibit a wavy
 373 shape possibly indicative of multiple components as mentioned above. More detailed analysis will
 374 be necessary to resolve this issue.

6. Conclusion

375
 376 The spectral properties of the LBAS blazars in the gamma-ray band, as determined over
 377 the first 6 months of LAT operation, have been presented. The average photon index of LBAS
 378 blazars are found to be $\Gamma=2.46$ for FSRQs, $\Gamma= 2.21$ for LSP-BLLacs, $\Gamma=2.13$ for ISP-BLLacs
 379 and $\Gamma=1.86$ for HSP-BLLacs, with an rms of 0.16-0.18. Spectral breaks have been observed to
 380 be common features in FSRQs (the break energy ranging from 1 to 10 GeV in the source frame
 381 for the brightest sources), and present also in some bright LSP-BLLacs. The different spectral
 382 features reported here represent challenges for theoretical models aiming at describing the blazar
 383 phenomenon. Although the fairly strong correlation between photon index and blazar class fits
 384 well within pictures (Ghisellini et al. 1998; Böttcher & Dermer 2002) where the cooling due to
 385 strong ambient radiation fields (manifesting themselves via the presence of emission lines) limits
 386 the acceleration of particles at high energy, the near constancy of this photon index with time and
 387 flux variation provides new constraints on the emitting particle dynamics. Moreover, the fact that
 388 spectra for most FSRQs and some LSP-BLLacs are best modeled by a BPL with a break in the
 389 1-10 GeV range is quite unexpected, the break representing a distinctive feature of these sources.
 390 The LAT has already revealed novel aspects of gamma-ray blazars and will help refine the new
 391 picture that progressively emerges as more data (both in the gamma-ray and other bands) are
 392 accumulated.

7. Acknowledgments

393
 394 The *Fermi* LAT Collaboration acknowledges generous ongoing support from a number of
 395 agencies and institutes that have supported both the development and the operation of the LAT as
 396 well as scientific data analysis. These include the National Aeronautics and Space Administration
 397 and the Department of Energy in the United States, the Commissariat à l’Energie Atomique and
 398 the Centre National de la Recherche Scientifique / Institut National de Physique Nucléaire et de
 399 Physique des Particules in France, the Agenzia Spaziale Italiana and the Istituto Nazionale di Fisica
 400 Nucleare in Italy, the Ministry of Education, Culture, Sports, Science and Technology (MEXT),
 401 High Energy Accelerator Research Organization (KEK) and Japan Aerospace Exploration Agency

³The low confidence association obtained with 3 months worth of data has by now turned into a high-confidence one for this source.

402 (JAXA) in Japan, and the K. A. Wallenberg Foundation, the Swedish Research Council and the
403 Swedish National Space Board in Sweden.

404 Additional support for science analysis during the operations phase is gratefully acknowledged
405 from the Istituto Nazionale di Astrofisica in Italy and the Centre National d'Études Spatiales in
406 France. *Facilities: Fermi* LAT.

REFERENCES

- 407
- 408 Abdo, A. A., et al. 2009a, ArXiv e-prints 0912.4029
- 409 —. 2009b, *Physical Review Letters*, 103, 251101
- 410 —. 2009c, *ApJS*, 183, 46
- 411 —. 2009d, *ApJ*, 699, 817
- 412 —. 2009e, *ApJ*, 700, 597
- 413 —. 2009f, ArXiv e-prints 0912.2040
- 414 Aharonian, F., et al. 2009, *ApJ*, 696, L150
- 415 Atwood, W. B., et al. 2009, *ApJ*, 697, 1071
- 416 Böttcher, M. 2007, *Ap&SS*, 309, 95
- 417 Böttcher, M., & Dermer, C. D. 2002, *ApJ*, 564, 86
- 418 D'Agostini, G. 2004, ArXiv Physics e-prints arXiv:physics/0403086
- 419 Dermer, C. D., & Schlickeiser, R. 1993, *ApJ*, 416, 458
- 420 Drury, L. O. 1991, *MNRAS*, 251, 340
- 421 Fichtel, C. E., et al. 1994, *ApJS*, 94, 551
- 422 Fields, B. D., Pavlidou, V., & Prodanović, T. 2008, in *International Cosmic Ray Conference*, Vol. 2,
423 *International Cosmic Ray Conference*, 153–156
- 424 Finke, J. D., Dermer, C. D., & Böttcher, M. 2008, *ApJ*, 686, 181
- 425 Ghisellini, G. 1989, *MNRAS*, 236, 341
- 426 Ghisellini, G., Celotti, A., Fossati, G., Maraschi, L., & Comastri, A. 1998, *MNRAS*, 301, 451
- 427 Ghisellini, G., Maraschi, L., & Tavecchio, F. 2009, *MNRAS*, 396, L105

- 428 Ghisellini, G., & Tavecchio, F. 2009, MNRAS, 397, 985
- 429 Hartman, R. C., et al. 1999, ApJS, 123, 79
- 430 —. 1992, ApJ, 385, L1
- 431 Kirk, J. G., & Mastichiadis, A. 1999, Astroparticle Physics, 11, 45
- 432 Marcha, M. J. M., Browne, I. W. A., Impey, C. D., & Smith, P. S. 1996, MNRAS, 281, 425
- 433 Mattox, J. R., et al. 1996, ApJ, 461, 396
- 434 Sikora, M., Begelman, M. C., & Rees, M. J. 1994, ApJ, 421, 153
- 435 Sreekumar, P., et al. 1998, ApJ, 494, 523
- 436 Stocke, J. T., Morris, S. L., Gioia, I. M., Maccacaro, T., Schild, R., Wolter, A., Fleming, T. A., &
437 Henry, J. P. 1991, ApJS, 76, 813
- 438 Strong, A. W., Moskalenko, I. V., & Reimer, O. 2004a, ApJ, 613, 962
- 439 Strong, A. W., Moskalenko, I. V., Reimer, O., Digel, S., & Diehl, R. 2004b, A&A, 422, L47
- 440 Urry, C. M., & Padovani, P. 1995, PASP, 107, 803
- 441 Vaughan, S., Edelson, R., Warwick, R. S., & Uttley, P. 2003, MNRAS, 345, 1271
- 442 Vercellone, S., et al. 2009, ApJ, 690, 1018
- 443 Vermeulen, R. C., Ogle, P. M., Tran, H. D., Browne, I. W. A., Cohen, M. H., Readhead, A. C. S.,
444 Taylor, G. B., & Goodrich, R. W. 1995, ApJ, 452, L5+
- 445 Webb, G. M., Drury, L. O., & Biermann, P. 1984, A&A, 137, 185

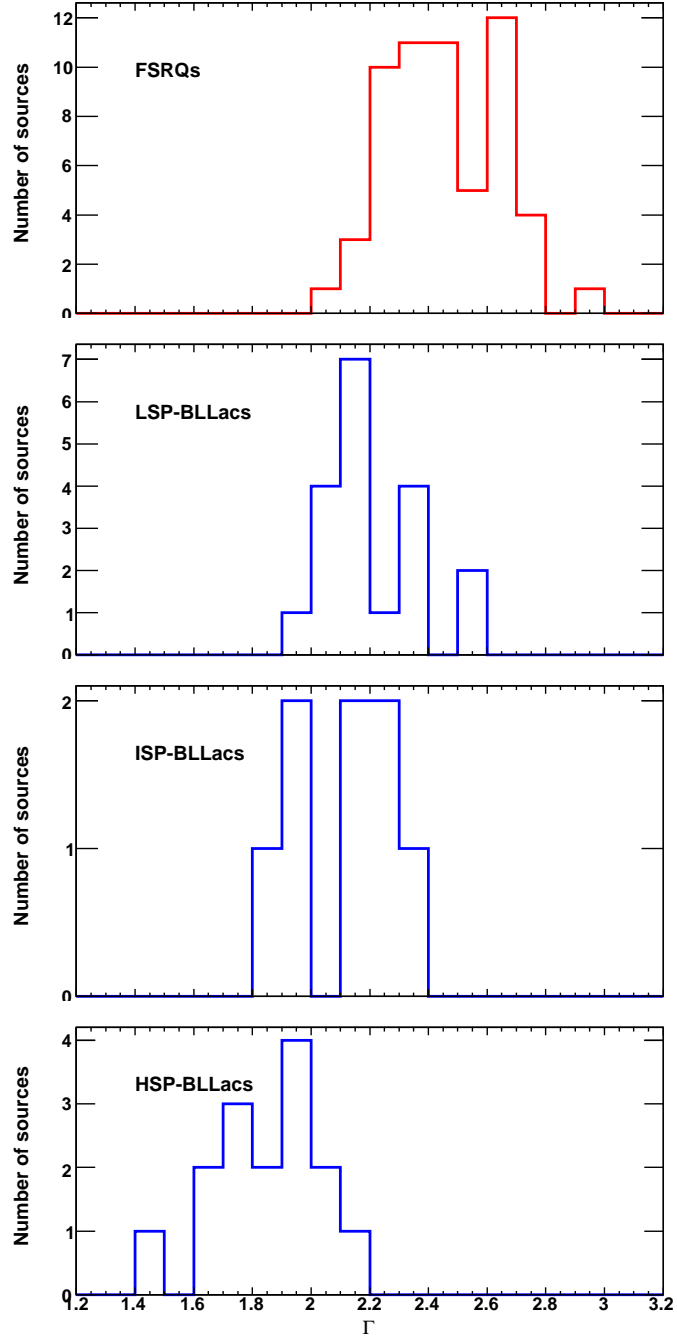


Fig. 1.— Gamma-ray photon index distributions for the four blazar subclasses.

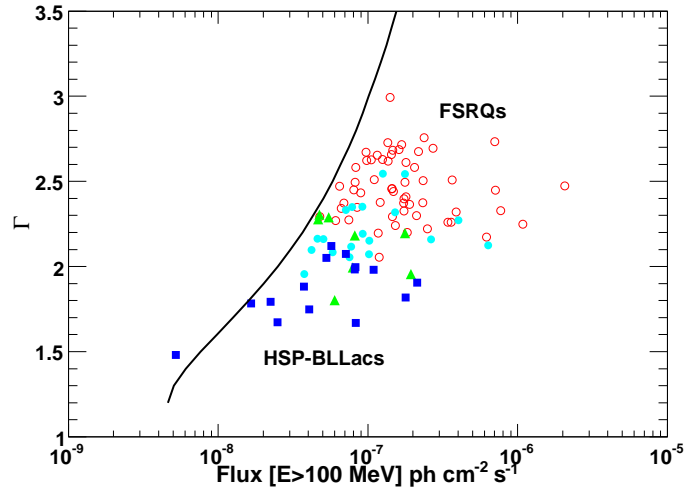


Fig. 2.— Photon index Γ vs Flux ($E > 100$ MeV) for the LBAS sources considered here. Open circles, red: FSRQs; solid symbols: BL Lacs (cyan circles: LSP-BLLacs, green triangles: ISP-BLLacs, blue squares: HSP-BLLacs). The solid curve represents the $TS = 100$ limit for a 3 month period (i.e. the defining condition of the LBAS sample) estimated for $(l,b)=(80^\circ, 40^\circ)$.

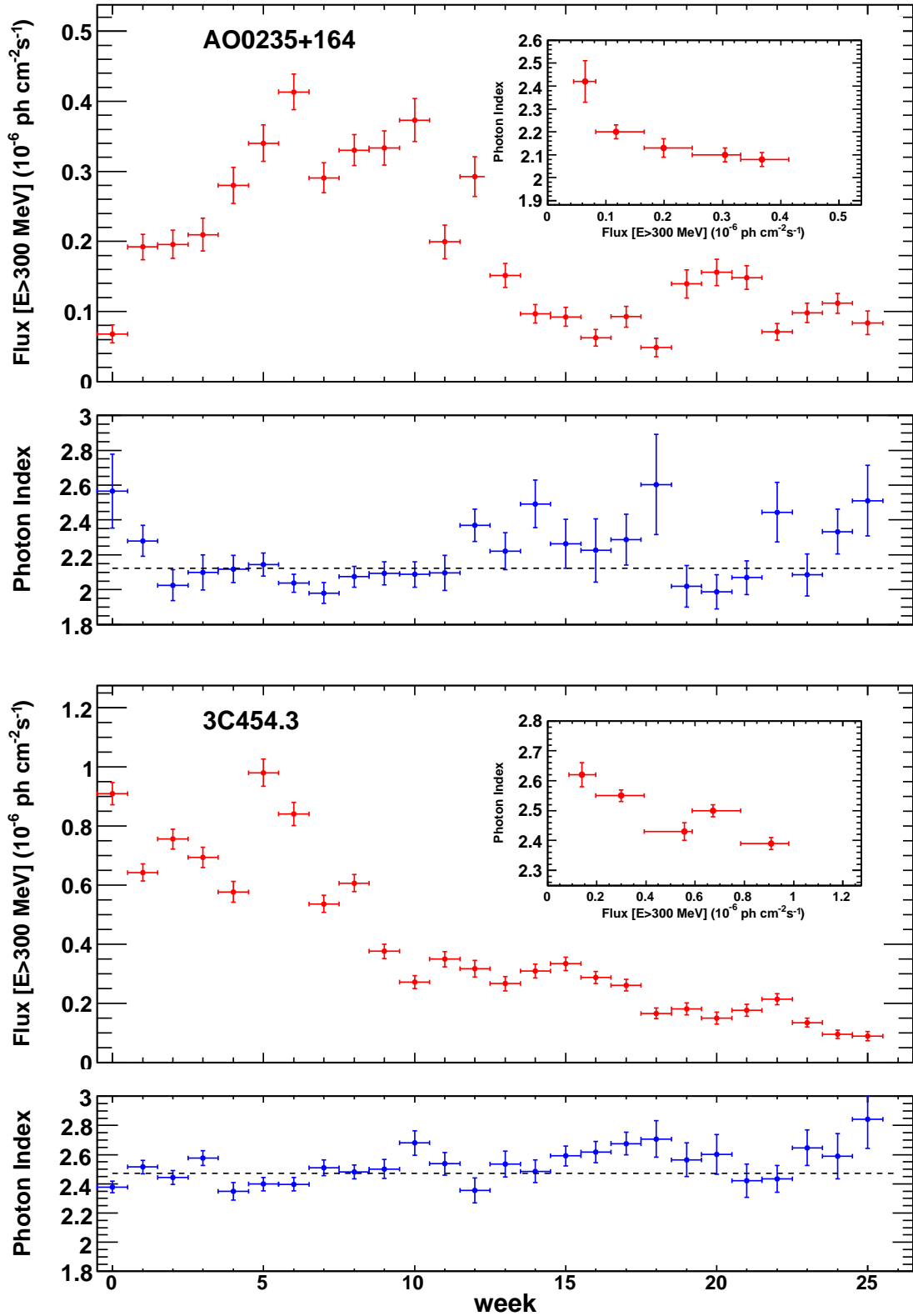


Fig. 3.— Measured weekly fluxes and photon index for 3C 454.3 and AO 0235+164 used as input of the simulations described in the text. The insets show the photon index resulting from an analysis where photons were sorted in five weekly-flux bins plotted vs the weekly flux.

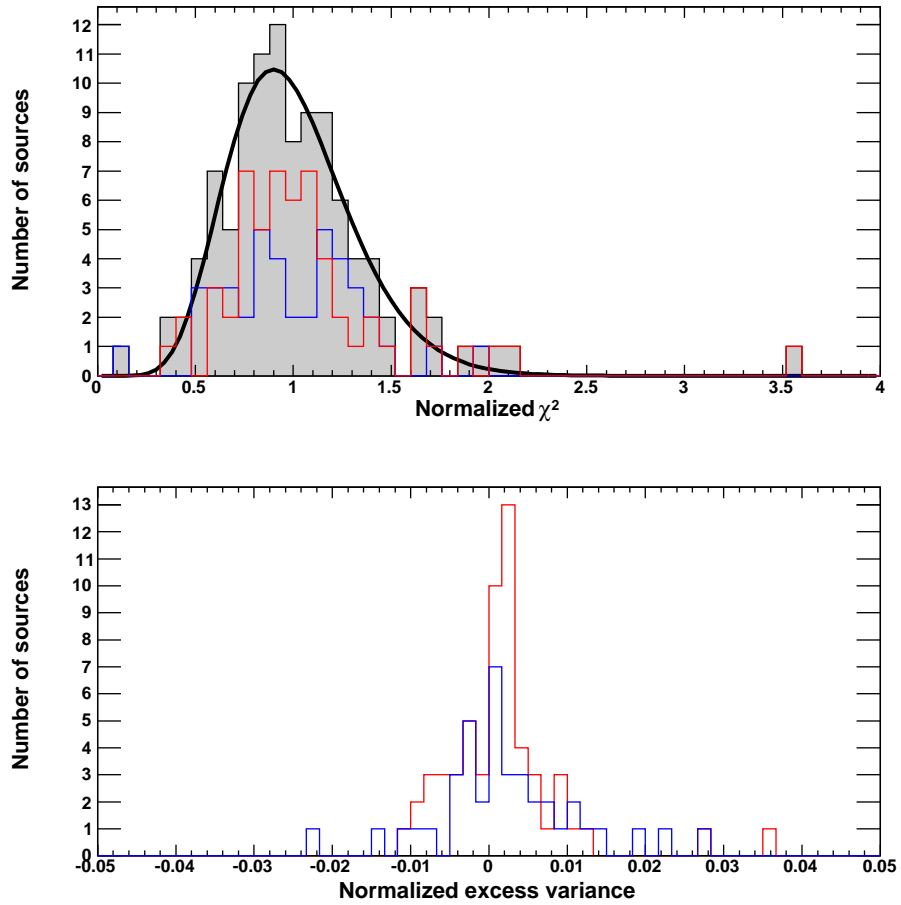


Fig. 4.— Top: Normalized χ^2 distributions of the weekly photon indices for FSRQs (red), BLLacs (blue) and all sources (black). Bottom: Normalized excess variance distributions of the weekly photon indices for FSRQs (red) and BLLacs (blue).

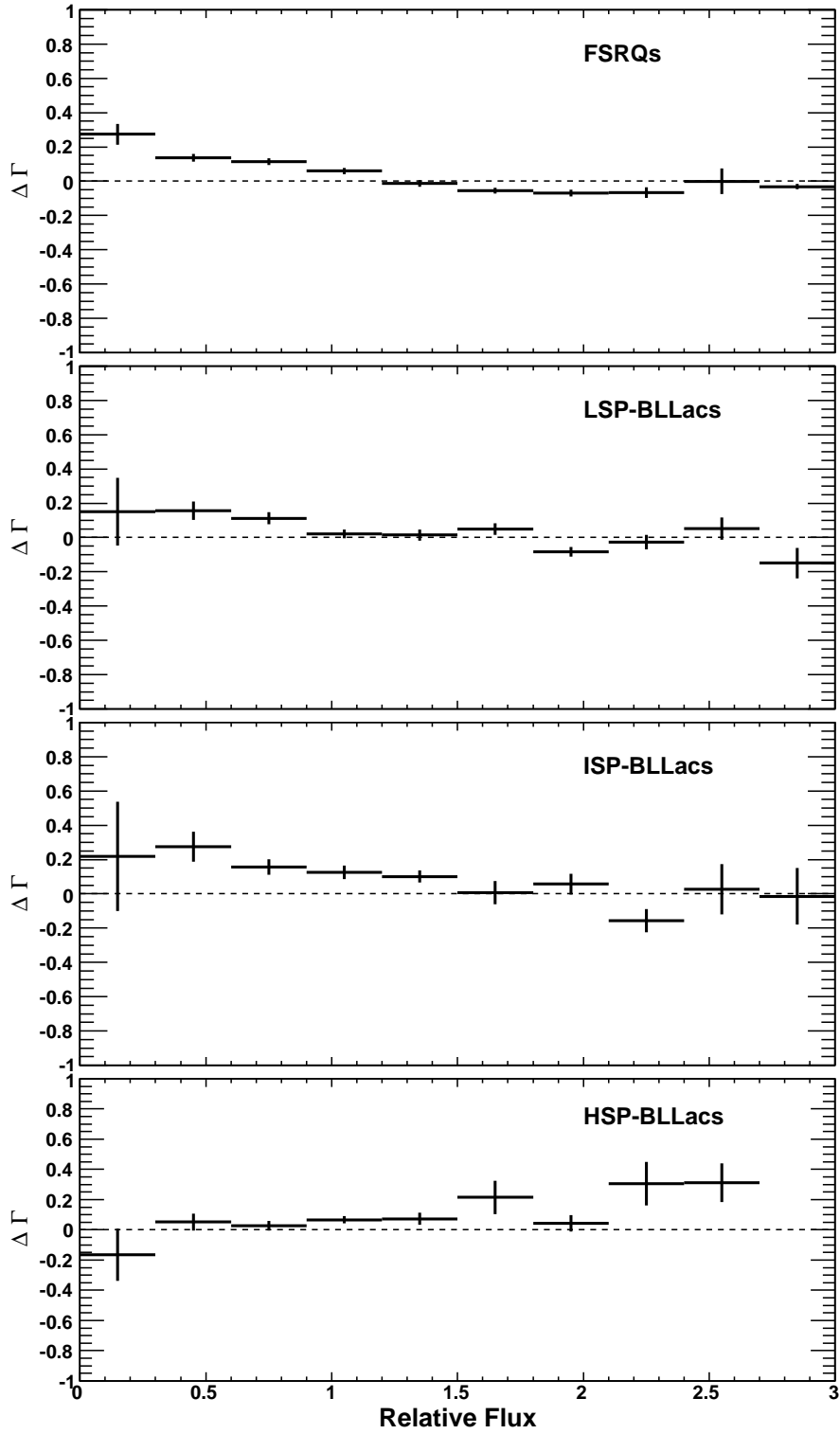


Fig. 5.— Average variation of photon index, Γ , vs relative flux (normalized to the average flux), for the different blazar subclasses. The data are integrated over a weekly timescale, and only the eight brightest representatives of each subclass have been considered.

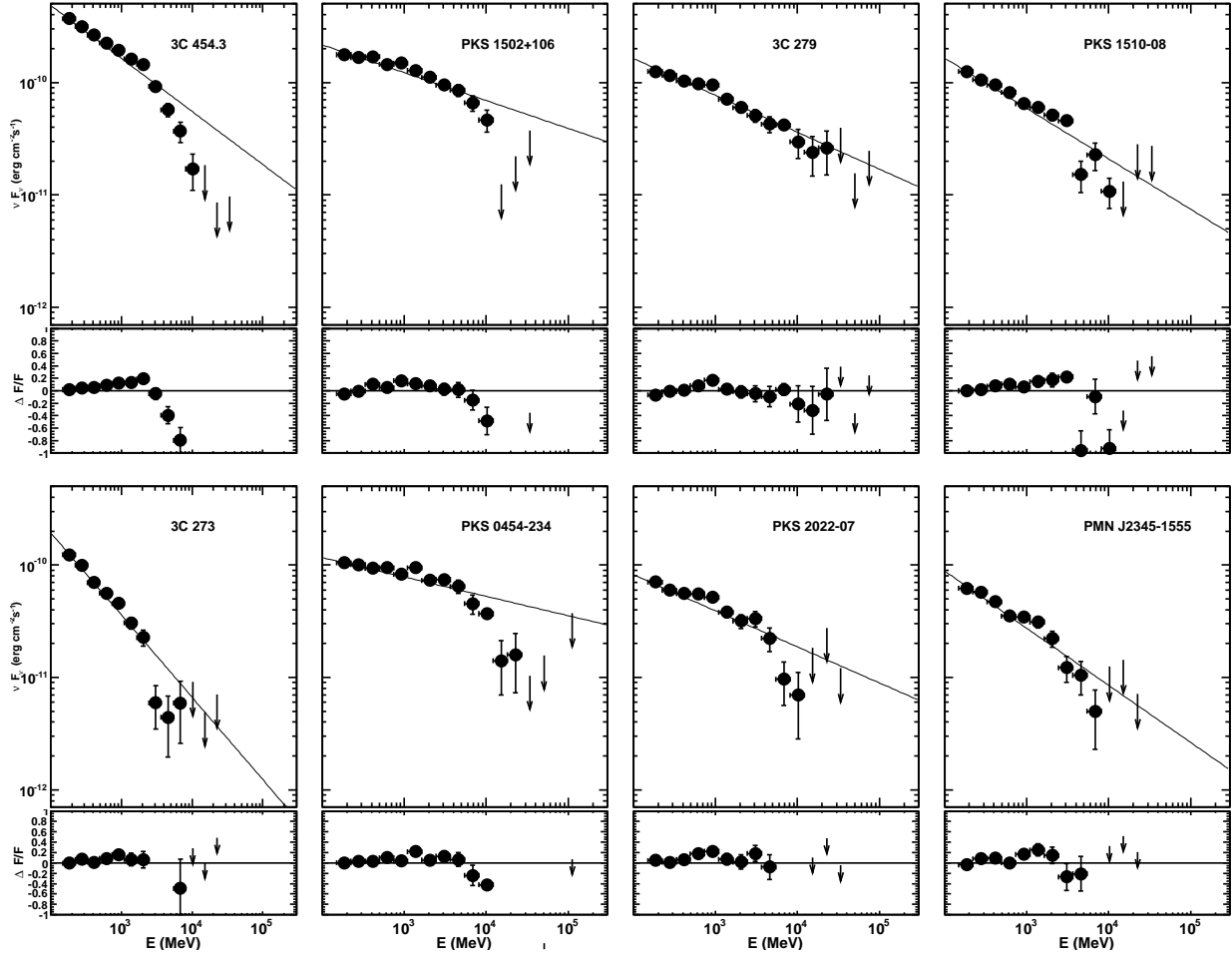


Fig. 6.— Gamma-ray spectra of the eight brightest FSRQs in the LBAS sample obtained for equispaced logarithmic bins (dots), together with residues with respect to the fitted power-law model (solid lines in upper panels).

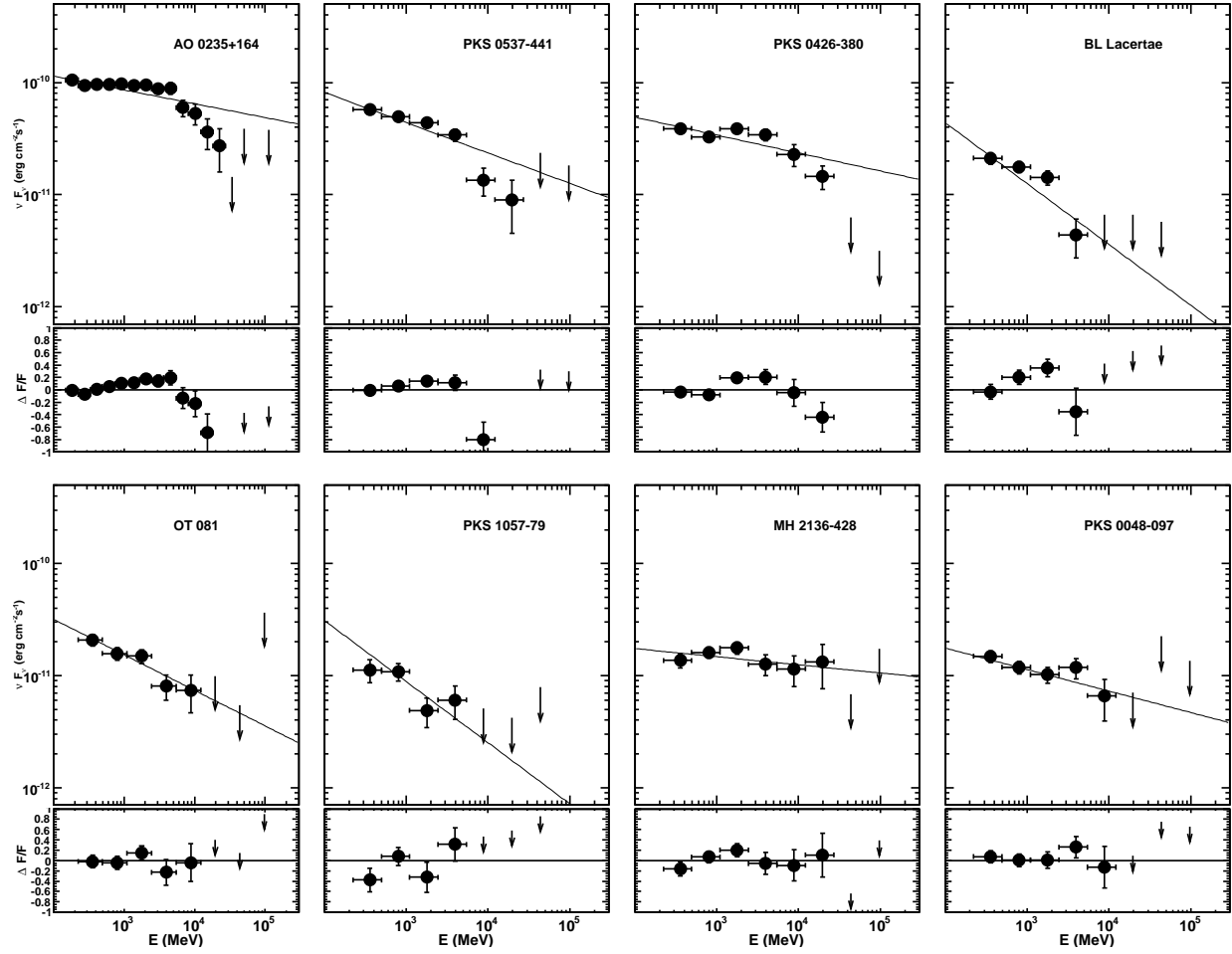


Fig. 7.— Same as Fig. 6, for the eight brightest LSP-BLLacs in the LBAS sample.

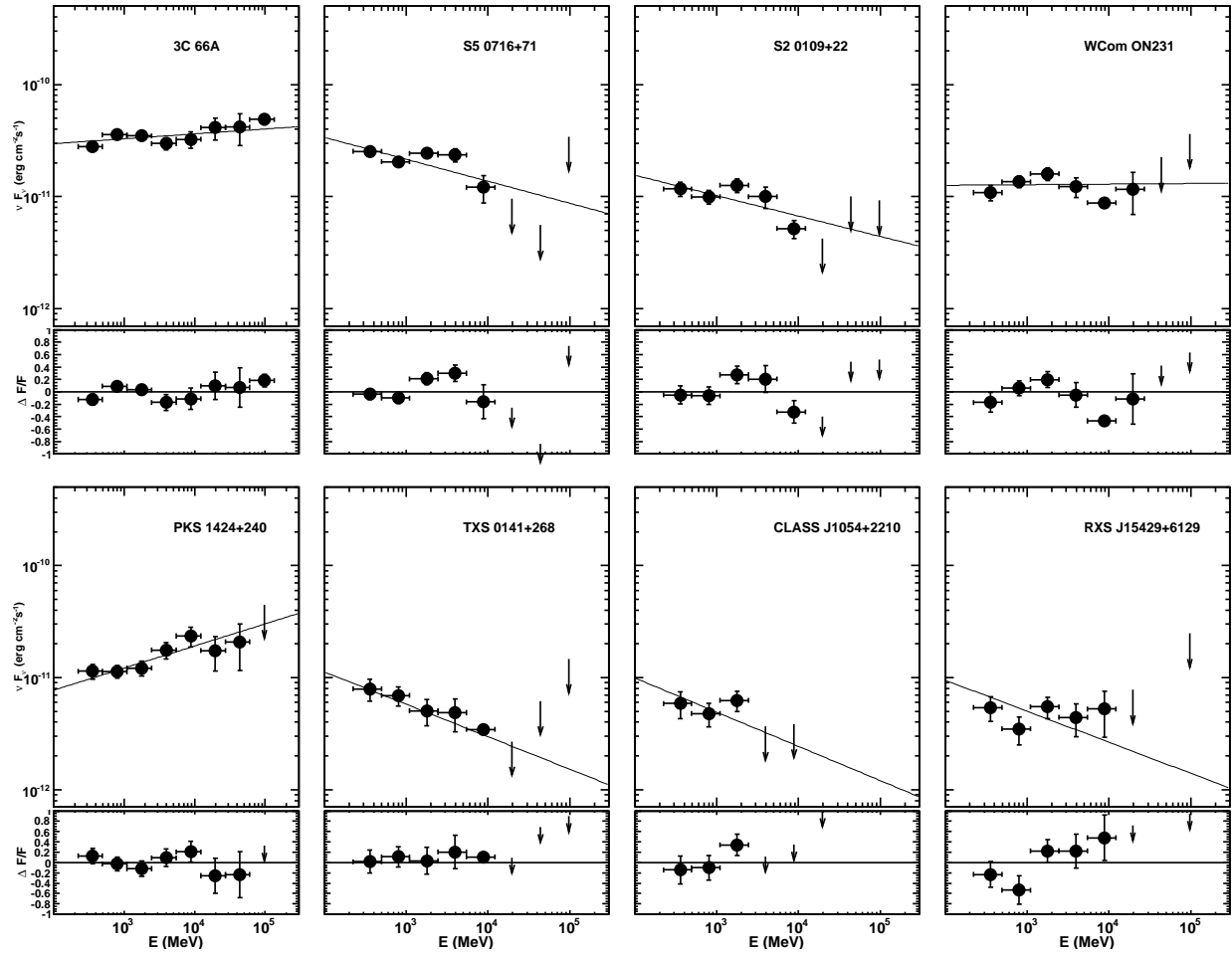


Fig. 8.— Same as Fig. 6, for the eight brightest ISP-BLLacs in the LBAS sample.

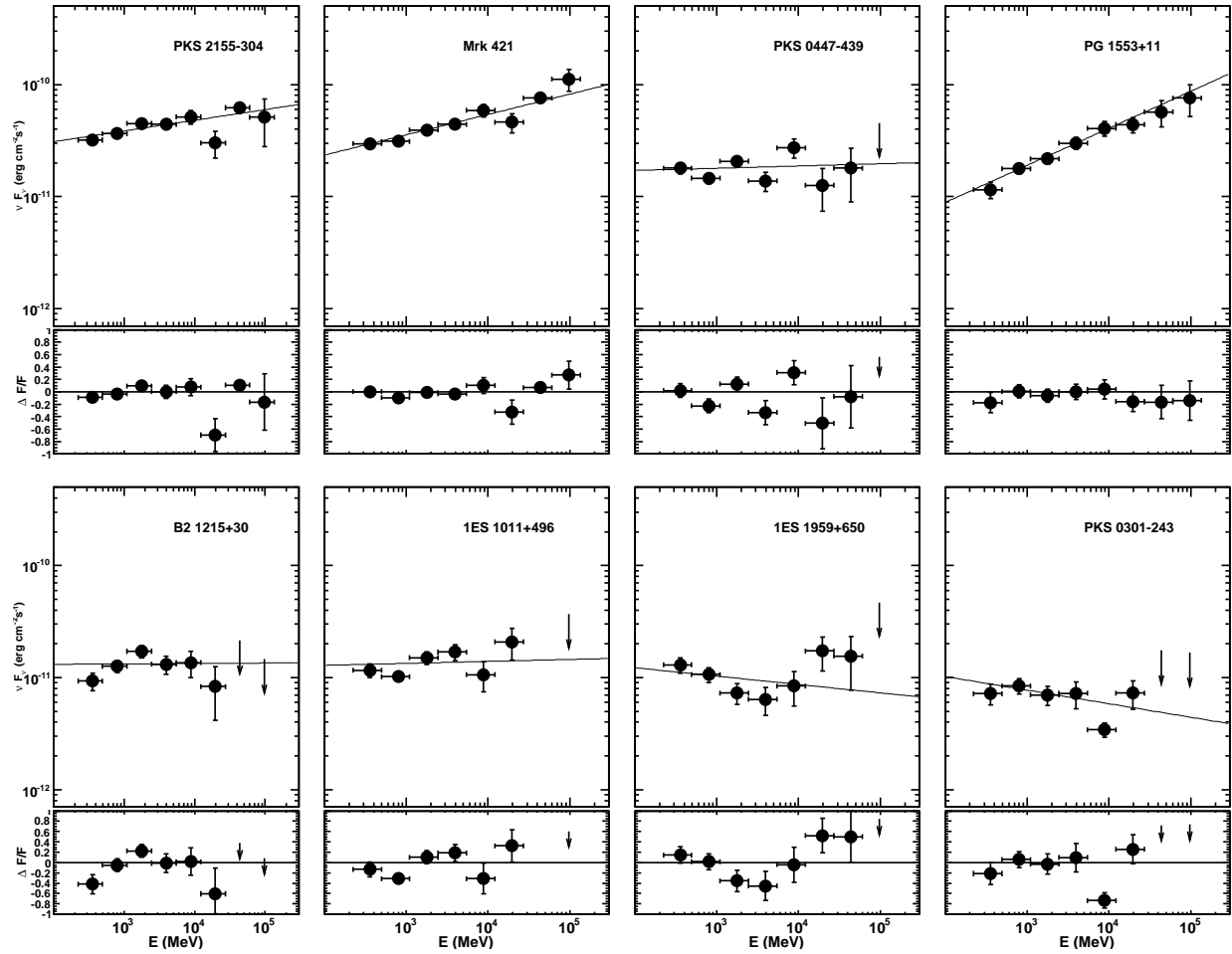


Fig. 9.— Same as Fig. 6, for the eight brightest HSP-BLLacs in the LBAS sample.

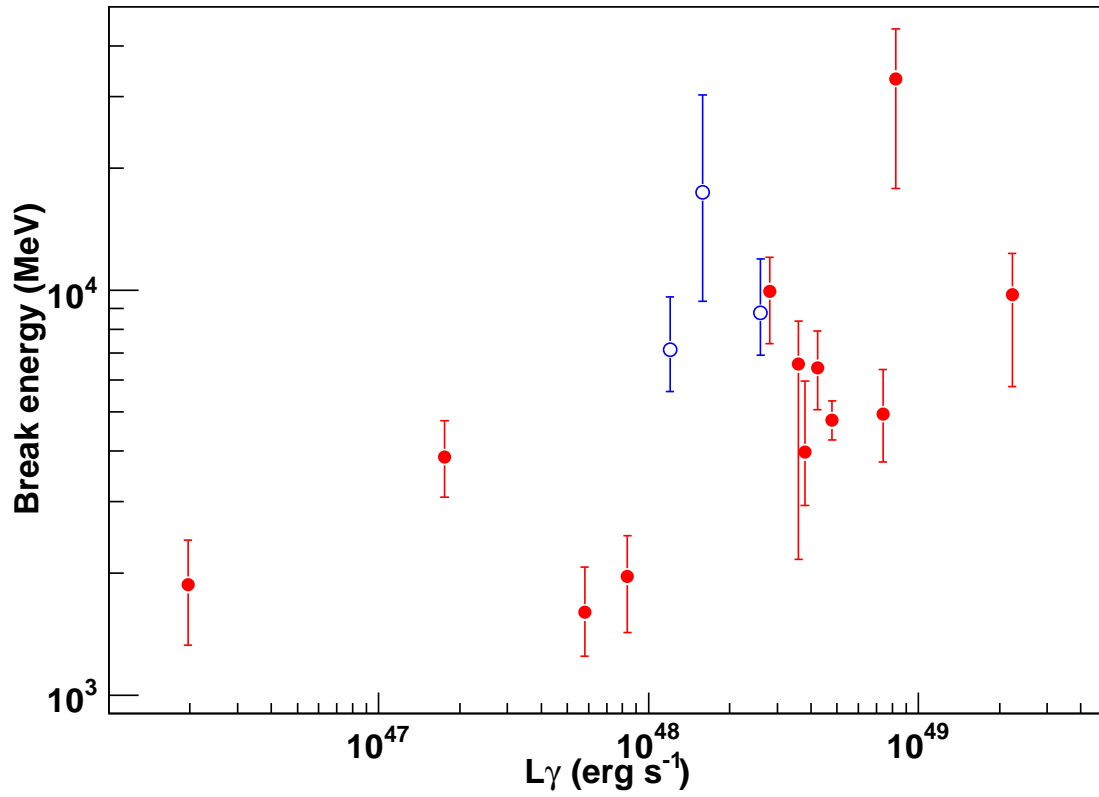


Fig. 10.— Break energy vs gamma-ray luminosity for the FSRQs (closed red symbols) and LSP-BLLacs (open blue symbols) listed in Table 1 and 2 respectively.

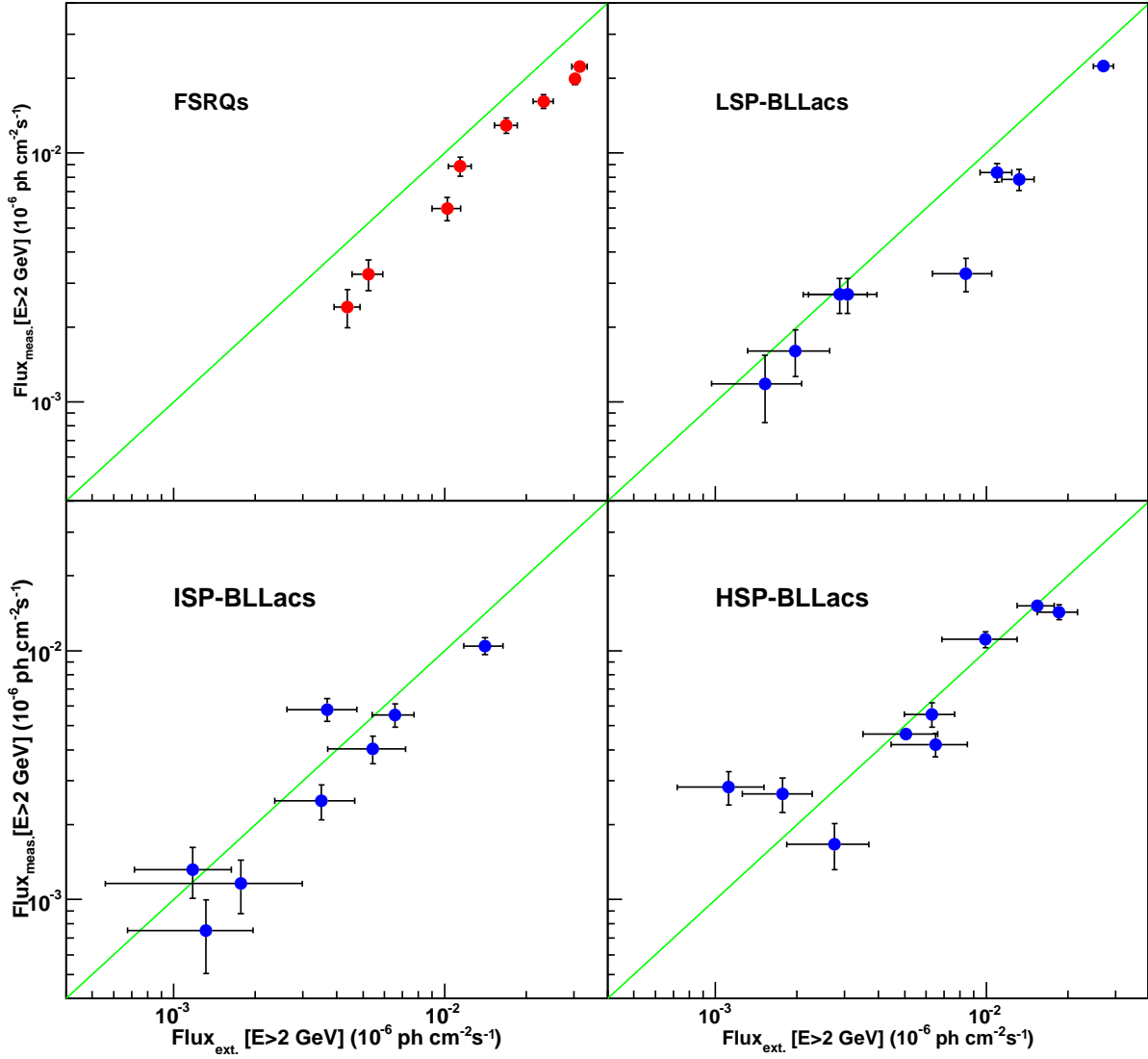


Fig. 11.— Measured vs extrapolated flux above 2 GeV for the eight brightest sources of each blazar subclass. The distance of the points from the diagonal is indicative of the presence of a spectral break.

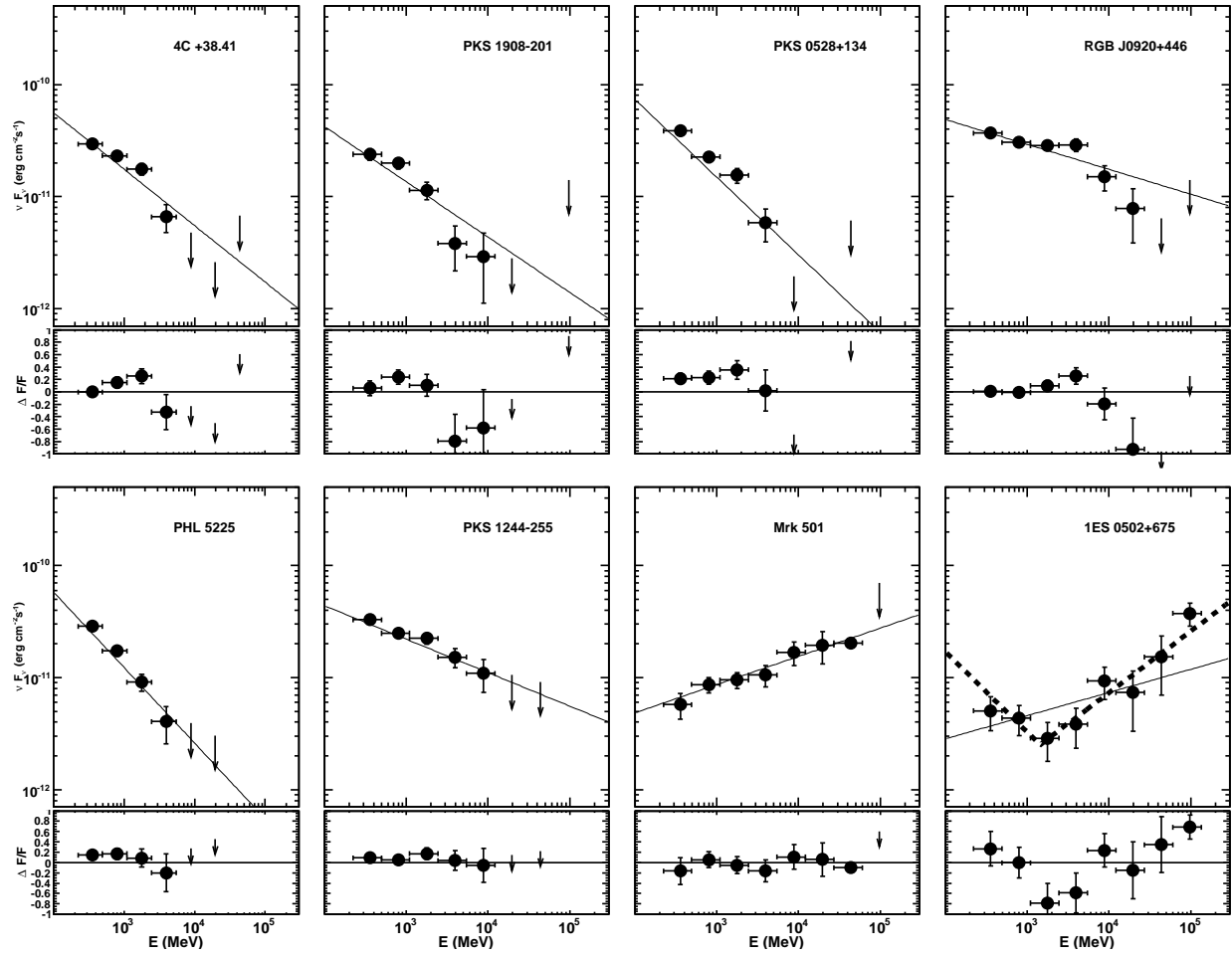


Fig. 12.— Same as Fig. 6, for eight particular sources in the LBAS sample.

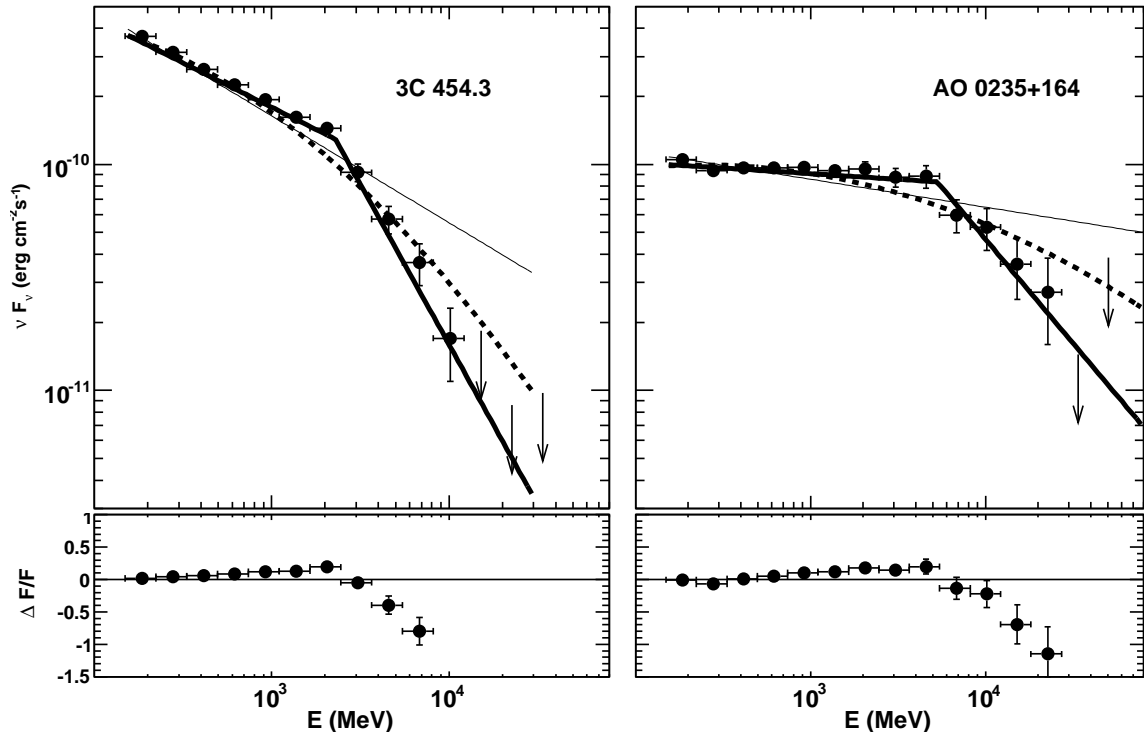


Fig. 13.— Upper panels: Energy spectra of 3C 454.3 (left) and AO 0235+164 (right) compared with fit results obtained with different models: PL (thin solid), BPL (thick solid) and logparabola (dashed).

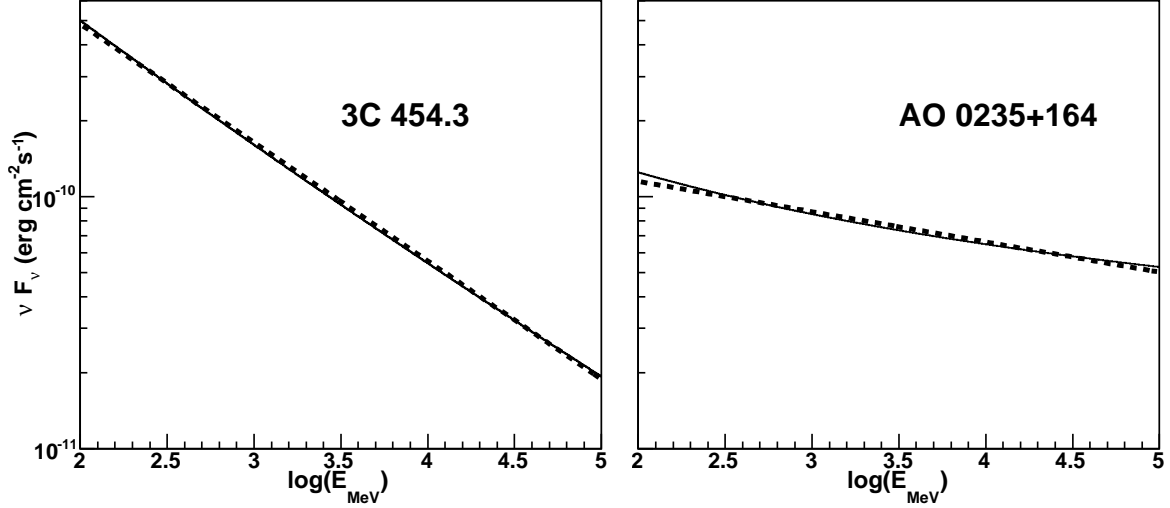


Fig. 14.— Analytical energy spectra (solid curves) of 3C 454.3 and AO 0235+164 resulting from summing power-law distributions with parameters (flux, photon index) as measured in weekly bins (Fig. 4). The dashed lines represent PL fits.

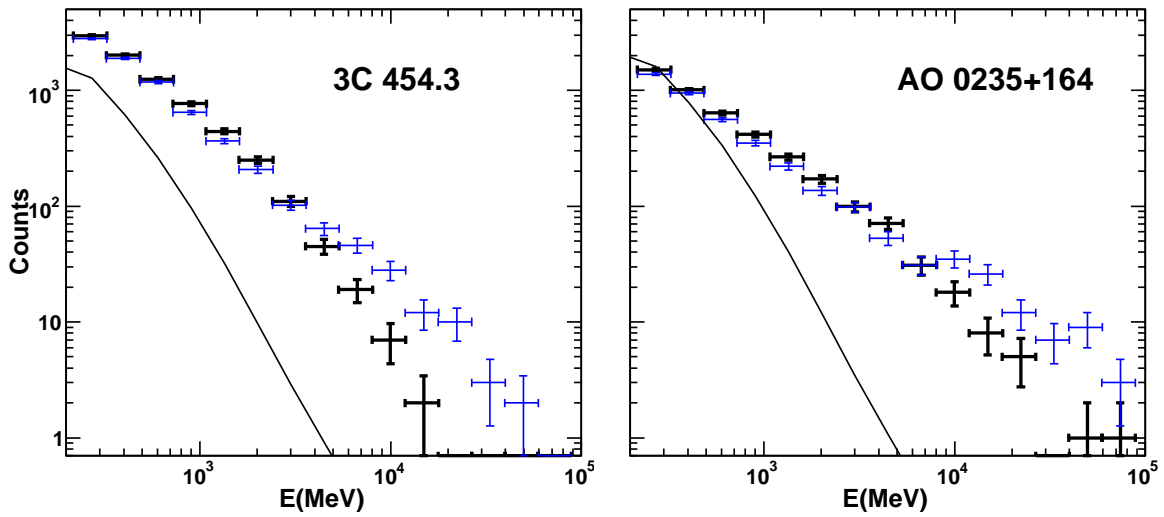


Fig. 15.— Count distributions within the 90% containment radius of simulated (blue, thin) and real (black, thick) data for 3C 454.3 and AO 0235+164. The solid curve correspond to the total contribution of galactic and isotropic diffuse backgrounds.

Table 1. Spectral properties of selected FSRQs

Name	l	b	Flux $_{PL}$ ^a	Γ	ΔL	Flux $_{BPL}$ ^a	Γ_1	Γ_2	$\Delta\Gamma$	E_{Break} (GeV)	z	E'_{Break} (GeV)	Luminosity ^b
3C 454.3	86.12	-38.1	2.053±0.02	2.47±0.01	-54.7	1.994±0.029	2.40±0.01	3.51±0.12	1.10±0.12	2.5 ^{+0.3} _{-0.3}	0.859	4.8 ^{+0.55} _{-0.55}	44.1
PKS 1502+106	11.37	54.58	1.068±0.02	2.24±0.01	-34.0	1.024±0.019	2.17±0.01	3.06±0.12	0.89±0.12	3.45 ^{+0.9} _{-0.15}	1.839	9.7 ^{+2.6} _{-0.4}	185
3C 279	305.1	57.06	0.754±0.01	2.32±0.02	-6.60	0.724±0.021	2.24±0.03	2.50±0.05	0.25±0.06	1.05 ^{+0.3} _{-0.2}	0.536	1.6 ^{+0.5} _{-0.3}	5.0
PKS 1510-08	351.2	40.13	0.739±0.02	2.47±0.02	-7.13	0.717±0.042	2.42±0.05	3.08±0.25	0.66±0.26	2.8 ^{+0.7} _{-0.6}	0.36	3.9 ^{+0.9} _{-0.8}	1.60
3C 273	289.9	64.36	0.682±0.02	2.73±0.03	-9.12	0.669±0.023	2.68±0.03	3.66±0.28	0.97±0.28	1.6 ^{+0.5} _{-0.5}	0.158	1.9 ^{+0.55} _{-0.55}	0.19
PKS 0454-234	223.7	-34.9	0.632±0.01	2.19±0.01	-23.5	0.604±0.016	2.11±0.02	3.28±0.21	1.16±0.21	4.95 ^{+1.1} _{-0.13}	1.003	9.95 ^{+2.1} _{-0.25}	22.1
PKS 2022-07	36.89	-24.3	0.439±0.01	2.38±0.03	-4.54	0.420±0.018	2.32±0.03	2.84±0.17	0.52±0.18	2.75 ^{+0.8} _{-0.18}	1.388	6.6 ^{+1.8} _{-0.45}	31.1
TXS 1520+319	50.14	57.04	0.381±0.01	2.52±0.03	-3.95	0.364±0.016	2.45±0.04	2.90±0.15	0.45±0.16	1.6 ^{+0.8} _{-0.4}	1.487	4.0 ^{+2.0} _{-0.1}	35.4
4C +38.41	61.08	42.40	0.229±0.01	2.50±0.04	-10.1	0.211±0.014	2.36±0.05	4.06±0.50	1.70±0.50	2.3 ^{+0.55} _{-0.5}	1.814	6.4 ^{+1.5} _{-0.15}	39.3
PKS 1908-201	16.89	-13.1	0.160±0.01	2.42±0.06	-9.31	0.143±0.018	2.09±0.13	3.18±0.22	1.09±0.25	0.9 ^{+0.25} _{-0.25}	1.119	1.95 ^{+0.55} _{-0.55}	7.75
PKS 0528+134	191.3	-11.0	0.309±0.02	2.72±0.05	-7.42	0.268±0.020	2.52±0.07	3.87±0.47	1.34±0.48	1.6 ^{+0.45} _{-0.4}	2.07	4.9 ^{+1.4} _{-1.2}	71.4
RGB J0920+446	175.7	44.82	0.247±0.01	2.22±0.03	-7.61	0.235±0.012	2.16±0.03	4.86±0.84	2.70±0.84	1.0 ^{+3.0} _{-0.5}	2.19	3.3 ^{+11.0} _{-1.5}	67.2

^a10⁻⁶ ph[E>100 MeV]cm⁻²s⁻¹

^b10⁴⁷ erg s⁻¹

Table 2. Spectral properties of selected BLLacs

Name	l	b	Flux _{PL} ^a	Γ	ΔL	Flux _{BPL} ^a	Γ_1	Γ_2	$\Delta\Gamma$	E_{Break} (GeV)	z	E'_{Break} (GeV)	Luminosity ^b
LSP-BLLacs													
AO 0235+164	156.7	-39.0	0.630±0.01	2.12±0.01	-20.8	0.599±0.016	2.04±0.02	2.80±0.12	0.75±0.13	4.5 ^{+1.5} _{-1.0}	0.94	8.8 ^{+3.0} _{-1.9}	19.6
PKS 0537-441	250.0	-31.0	0.400±0.01	2.28±0.02	-8.51	0.380±0.015	2.20±0.03	3.08±0.23	0.87±0.24	3.8 ^{+1.3} _{-0.8}	0.892	7.1 ^{+2.5} _{-1.5}	10.1
PKS 0426-380	240.7	-43.6	0.274±0.01	2.18±0.03	-7.17	0.255±0.012	2.10±0.03	3.36±0.45	1.26±0.45	8.3 ^{+6.0} _{-0.4}	1.112	17.5 ^{+13.0} _{-0.8}	12.3
HSP-BLLac													
1ES 0502+675	143.7	15.89	0.019±0.00	1.70±0.14	-8.40	0.064±0.015	2.68±0.18	1.47±0.10	-1.2±0.21	1.4 ^{+0.7} _{-0.5}	0.416	2.0 ^{+1.0} _{-0.7}	0.12

^a10⁻⁶ ph[E>100 MeV]cm⁻²s⁻¹

^b10⁴⁷ erg s⁻¹